

Effect of transverse magnetic fields on high harmonic generation in intense laser-solid interaction

Jie Mu¹, Fei-Yu Li², Zheng-Ming Sheng^{1,2,*} and Jie Zhang¹

¹ *Key Laboratory for Laser Plasmas (MoE) and Department of Physics and Astronomy,
Shanghai Jiao Tong University, Shanghai 200240, China and*

² *SUPA, Department of Physics, University of Strathclyde, Glasgow G4 0NG, UK*

(Dated: June 20, 2016)

Abstract

The effect of transverse magnetic fields on surface high harmonic generation in intense laser-solid interactions is investigated. It is shown that the longitudinal motion of electrons can be coupled with the transverse motion via the magnetic fields, which lead to even-order harmonics under normal laser incidence. The dependence of the coupling efficiency and hence even harmonic generation with preplasma scalelength and magnetic field strength are presented based upon particle-in-cell simulations. When the magnetic field is parallel to the laser electric field, the spectral intensity of the second harmonic is proportional to the magnetic field strength in a wide range up to 160MG, while the situation with the magnetic field perpendicular to the laser electric field is more complicated. The second harmonic generation due to the magnetic field also tends to increase with the plasma density scalelengths, which is different from the high harmonics generation by the oscillating mirror mechanism. With the increase of the laser spot size from a laser wavelength λ_L , both the magnetic field induced harmonics and oscillating mirror high harmonics tend to increase first and then become saturated after $3\lambda_L$. The magnetic field induced second harmonic may be used to evaluate large self-generated magnetic fields developed near the critical density region and the preplasma conditions.

Keywords: high harmonics generation, magnetic field, laser-plasma interaction

INTRODUCTION

High harmonic generation in intense short-pulse laser interaction with solid targets contains rich information of the instantaneous dynamics that are deeply rooted in the highly nonlinear process. It thus has led to diverse applications such as measuring the hole-boring speed for fast ignition researches (Zepf *et al.*, 1996; Weng *et al.*, 2015) and sensing megagauss (MG) magnetic fields in solids heated by intense lasers (Tatarakis *et al.*, 2002). Another major application is to produce extremely short light pulses down to attoseconds (Mairesse *et al.*, 2003; Foldes *et al.*, 2003). Solid surface harmonics can provide intense enough attosecond pulses for probing ultrafast dynamics within the atomic timescale (Tsakiris *et al.*, 2006). **Polarization gating is used as a control of surface oscillations of solid targets to produce isolate attosecond pulses (Yeung *et al.*, 2015).**

In surface high harmonic generation (SHHG), an intense laser pulse is reflected by relativistically oscillating layers of surface electrons driven by the laser pulse itself (Bulanov *et al.*, 1994; Lichters *et al.*, 1996). Under normal incidence, the reflected pulses contain only odd harmonics polarized in parallel to the drive pulse, which have been modeled using a sharp vacuum-plasma interface and follows the well-known selection rules (Lichters *et al.*, 1996). In practice, additional conditions will also contribute, the first being preplasma expansion attributed to electron pre-heating arising from either the rising edge of incident pulses, prepulses, or a second pulse sent prior to the main pulse (Macphee *et al.*, 2010; Ma *et al.*, 2012). The efficiency of SHHG was found to be sensitive to the preplasma scale length (Ozaki *et al.*, 2007), dramatically enhanced in certain range because of a lower density involved and deteriorated again for longer expansion (Dollar *et al.*, 2013; Kahaly *et al.*, 2013). The density gradient also plays a key role in the harmonic generation mechanism of coherent wake emission (Quéré *et al.*, 2006; Sheng *et al.*, 2005). The fine control of preplasma expansion has become a critical step towards efficient SHHG.

Additional complexity of SHHG may also come from self-generated magnetic fields. Quasi-static magnetic fields of 100 MG are shown to exist in the near-critical density region of solids via laser ponderomotive heating (Sudan, 1993; Mason & Tabak, 1998) as well as fast electron current. Typically these fields are along the azimuthal direction for laser normal incidence and are important to a number of processes such as laser absorption, laser driven ion acceleration, and fast electron transport (Stambulchik *et al.*, 2007). Potentially, such

quasi-static magnetic fields can also affect SHHG, which has not been clarified completely. In magnetized plasmas, the conversion of a fraction of a laser beam to its phase-mismatch second and third harmonics was analyzed with single particle model (Ghorbanalilu & Mohammad, 2012). It was also suggested that the coupling between the laser-driven oscillations and electron cyclotron motion in such magnetic fields can generate sidebands in the vicinity of harmonics (Zheng *et al.*, 2002).

In this paper, we explore the effect of high transverse magnetic fields on SHHG using particle-in-cell (PIC) simulations. The full process should incorporate target expansion and magnetic field generation due to pre-heating in picoseconds and subsequent high harmonic generation through femtosecond main pulse interactions. Here, we simplify the treatment by combining a clean femtosecond drive pulse, an external magnetic field of over 10MG transverse to the laser direction and a pre-defined preplasma region. **This can be used to mimic some conditions of relativistic laser-solid interaction under which high quasi-static magnetic fields at tens of MG level might exist, even though such high fields are currently not possible in laboratory with conventional technologies.** As we shall see, the presence of transverse magnetic fields alters appreciably the electron dynamics near the target surface due to the cyclotron motion. Coupling with surface longitudinal oscillations, they lead to even-order harmonics for simple normal-incidence geometry. In particular, when the magnetic field is parallel to the direction of the laser electric field, the intensity of these even harmonics shows well-behaved dependence with the magnitude of the exerted magnetic field strength, readily observable in experiments. **Thus, these results may not only allow the dynamic evolution of self-generated magnetic fields in the relativistic laser-solid interaction to be diagnosed via a pump-probe scheme, but also provide an active monitoring of surface dynamics by exerting a transverse magnetic field even if just at a few Tesla.**

THEORY MODEL

Qualitatively, the effect of a transverse magnetic field on the surface motion of electrons and subsequent SHHG can be sketched with Fig. 1. Assume a linearly-polarized short intense laser pulse propagates along x direction and normally irradiates onto a foil target, which is placed under a uniform transverse magnetic field $\mathbf{B}_0 = B_{0y}\hat{y} + B_{0z}\hat{z}$, as shown in Fig. 1(a). It is well-known that electrons under the laser interaction will experience transverse

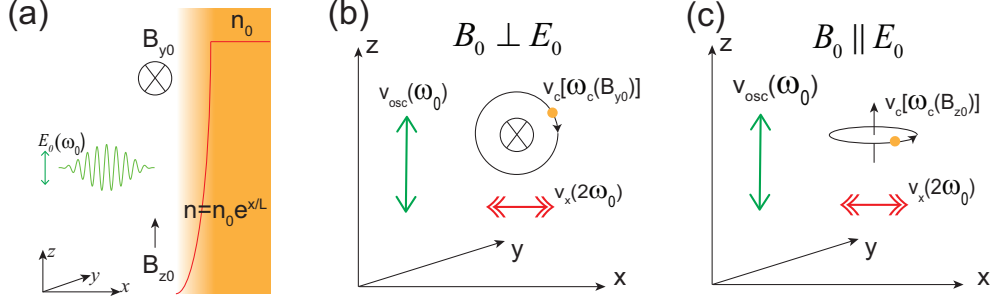


FIG. 1. (a) Sketch of the interaction configuration with the incident laser along the x direction and polarized along the z direction. (b) and (c) illustrate electron motion near the target surface under the interaction of incident laser and the transverse magnetic field either perpendicular or parallel to the laser electric field, respectively.

oscillation along the laser electric field along the z direction at the laser frequency ω_0 and the longitudinal oscillation along the x direction at $2\omega_0$, which form the xz plane. The coupling of longitudinal and transverse oscillations only leads to odd harmonics with the same polarization of the driving laser. When there is a transverse magnetic field \mathbf{B}_0 , these oscillations will couple with the cyclotron motion. In the case when this magnetic field is perpendicular to the laser electric field as shown in Fig. 1(b), the cyclotron motion will be within the xz plane. Therefore a new surface current component along the z direction at $2\omega_0$ will appear. As a result, both odd and even harmonics will be produced with the same polarization of the driving laser, which is different from the case without the magnetic field. On the other hand, when this magnetic field is parallel to the laser electric field as shown in Fig. 1(c), the cyclotron motion will be in a plane perpendicular to the xz plane. Therefore a new surface current component along the y direction at $2\omega_0$ will appear. As a result, even harmonics polarized long the y direction will be produced, while only odd harmonics with the same polarization of the driving laser.

Mathematically, the above scenario can be described by the equation of electron motion coupled with the Maxwell's equations. Under both the laser and magnetic fields, the equation of motion reads

$$\frac{d\mathbf{p}}{dt} = -e[\mathbf{E} + \mathbf{v} \times (\mathbf{B} + \mathbf{B}_0)], \quad (1)$$

where \mathbf{p} , \mathbf{v} and $-e$ are, respectively, the electron momentum, velocity, and charge of electrons, $\mathbf{E} = -\partial\mathbf{A}/\partial t - \nabla\phi$, $\mathbf{B} = \nabla \times \mathbf{A}$, ϕ is the electrostatic potential and $\mathbf{a} = e\mathbf{A}/m_e c$

is the normalized laser vector potential with m_e and c being the electron mass and light speed in vacuum. By combining Eq. (1) and the Maxwell's equations, the polarized vector potentials a_y (p polarized) and a_z (s polarized) satisfy the following wave equations,

$$\begin{aligned}(\partial_x^2 - \frac{1}{c^2}\partial_t^2)a_y &= (\frac{\omega_p}{c})^2 s_y, \\(\partial_x^2 - \frac{1}{c^2}\partial_t^2)a_z &= (\frac{\omega_p}{c})^2 s_z,\end{aligned}\tag{2}$$

with the source terms

$$\begin{aligned}s_y &= n\sqrt{1 - \beta_x^2}\frac{a'_y}{\sqrt{1 + a_y'^2 + a_z'^2}}, \\s_z &= n\sqrt{1 - \beta_x^2}\frac{a'_z}{\sqrt{1 + a_y'^2 + a_z'^2}}.\end{aligned}\tag{3}$$

Here, $a'_y = a_y + \frac{eB_{0z}}{m} \int_t \beta_x dt$ and $a'_z = a_z - \frac{eB_{0y}}{m} \int_t \beta_x dt$ with β_x being the longitudinal electron velocity normalized by c , $\omega_p = \sqrt{n_0 e^2 / m \varepsilon_0}$ is the plasma frequency defined by the maximum initial electron density n_0 , n is the electron density normalized by n_0 , and ε_0 is the vacuum permittivity.

The above equations reduce to that derived in Ref. (Lichters *et al.*, 1996) for $B_{0y} = B_{0z} = 0$. For example, for an s-polarized drive laser pulse, both the density fluctuation n and longitudinal velocity β_x contain only even-order harmonics of the laser frequency ω_L . Coupling with transverse laser oscillations, they lead to only odd harmonics polarized in the same plane as the drive pulse. While for nonzero \mathbf{B}_0 , the presence of the magnetic field modifies the vector potentials in the source terms with an additional terms $\frac{eB_{0z}}{m} \int_t \beta_x dt$ and $-\frac{eB_{0y}}{m} \int_t \beta_x dt$. Obviously, the additional terms are due to the cyclotron motion exerted by the magnetic field and the surface longitudinal oscillations β_x . In particular, additional even harmonics polarized orthogonal to the magnetic field, apart from the typical odd harmonics polarized in parallel to the drive pulse. Despite this simple qualitative analysis, the dependence of the even harmonic generation with laser-target and magnetic field parameters are quite complicated as the cyclotron motion and longitudinal oscillation are strongly coupled with each other. The cyclotron motion spreads over the entire region while density oscillation is most efficient only near the critical density surface. Under sufficient strong magnetic field, the cyclotron motion can also modify the surface oscillations. In the following, we adopt particle-in-cell (PIC) simulations to elucidate the details and provide parametric studies of this phenomenon.

NUMERICAL SIMULATION RESULTS

One-dimensional particle-in-cell simulation

We start with one-dimensional (1D) PIC simulations using the OSIRIS code (Fonseca *et al.*, 2002). The simulation box is initialized as $40\lambda_L$ long, divided into 4000 cells with 100 micro-particles per cell, where λ_L is the incident laser wavelength. The solid target is uniform in $x \in [0, 2\lambda_L]$, with a preplasma attached in the front varying as $n = n_0 \exp(x/L)$ where $n_0 = 40n_c$ is the peak density, $n_c = 1.1 \times 10^{21} \text{ cm}^{-3}$ is the critical density for $\lambda_L = 1 \mu\text{m}$, and $L = 0.2$ is the preplasma scale length. A linearly polarized laser pulse with normalized vector potential $a = a_0 \sin^2(\pi t/T_L)$ impinges from the left onto the target, where $a_0 = 0.5$ corresponds to a peak intensity of $3.4 \times 10^{17} \text{ W/cm}^2$, $\tau = 9T_L$ is the full pulse duration, and $T_L = 2\pi/\omega_0$ is the laser period. For clarity, we assume it is polarized along the z -direction and call it s -polarized. Ions are treated to be stationary background as they have little effect in this ultrafast process (Brügge *et al.*, 2012).

The reflected pulses are traced at $x = -4$ and the results (both time and frequency domains) are shown in Fig. 2 for different runs with or without external magnetic field in different directions. In the case without external magnetic field, only odd harmonics show up in s polarization and no harmonics is observed in p polarization, as shown by the black dashed lines in Figs. 2(a), 2(b) and 2(d), as expected in accordance with the selection rules (Lichters *et al.*, 1996). The prominent new feature occurs for $B_{0z} = 17 \text{ MG}$, where a well-defined reflected pulse containing even-order laser harmonics now emerges in p -polarization as shown in Fig. 2(c). The even-order harmonics occur in s -polarization for $B_{0y} = 17 \text{ MG}$, as shown in Fig. 2(d). The parity of these even harmonics changes with the direction of the external magnetic field and they are always perpendicular to the magnetic field, a clear evidence of electron cyclotron motion as theoretically discussed above. The merit of employing parallel magnetic field and incident laser field is that the even harmonics can be well separated from the reflection of the drive pulse due to their different polarizations.

The harmonics generation due to the magnetic field is also reflected in the transverse currents, which are actually the source terms give in Eq. (2). In Fig. 3, the electric current components j_y and j_z in different simulation runs with the transverse magnetic field either perpendicular or parallel to the laser electric field are shown in the spacetime plots. With

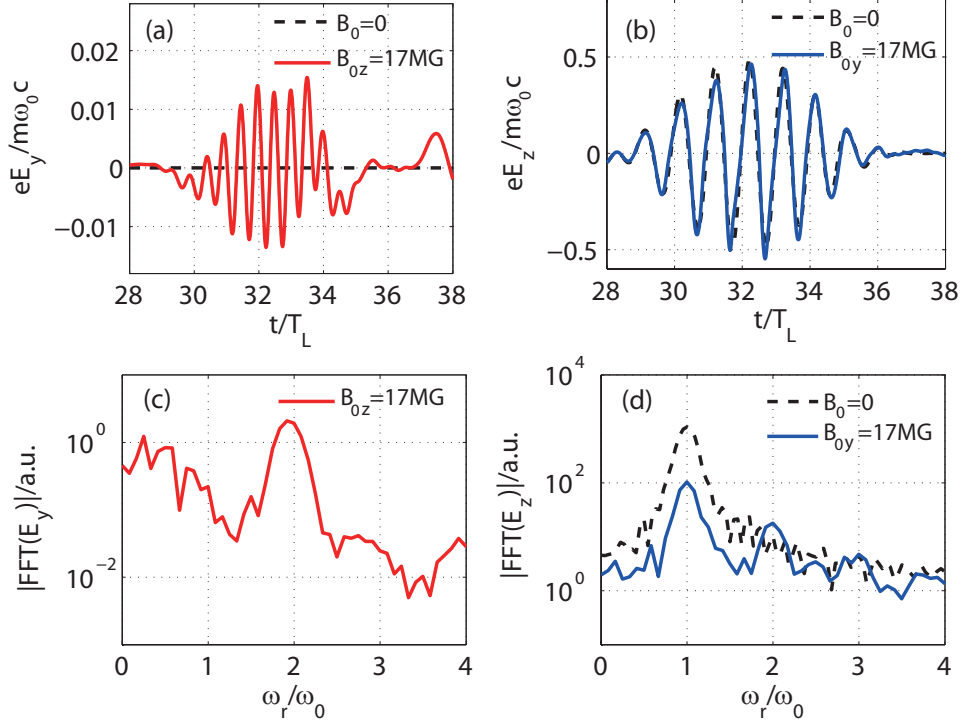


FIG. 2. (Color online) An s-polarized laser pulse is reflected by a solid target in different runs without and with a homogeneous magnetic field applied either in y - or z -directions. The p- and s-polarized components of the reflected electric field without the effect of magnetic field are plotted in black dashed lines in (a) and (b). The p-polarized component of the reflected electric field E_y in $B_{0z} = 17\text{MG}$ and its Fourier transformed spectra are shown in red solid lines in (a) and (c). The s-polarized component of the reflected electric field E_z in $B_{0y} = 17\text{MG}$ and its Fourier transformed spectra are shown in blue solid lines in (b) and (d).

the presence of magnetic field $B_{0z} = 17\text{MG}$, a new surface current j_y at $2\omega_0$ appears as shown in Fig. 3(a), resulting in the even harmonics in $|FFT(E_y)|$ shown in Fig. 2(c). Note that there is a low frequency current component near $x/\lambda_L \sim -1$ in Fig. 3(a), which can be attributed to the zero frequency component of the laser ponderomotive force and the charge separation fields at the front surface. The latter can drive longitudinal motion of electrons, which, when bended by B_{0z} , leads to low frequency transverse currents j_y finally. The electric current component j_z shown in Fig. 3(b) is dominated by oscillations at ω_0 , even though it contains odd harmonic components. Also note that the amplitude of j_z is an order of magnitude higher than the amplitude of j_y . With the presence of magnetic field $B_{0y} = 17\text{MG}$, there is simply $j_y = 0$. The electric current component j_z shown in Fig. 3(c)

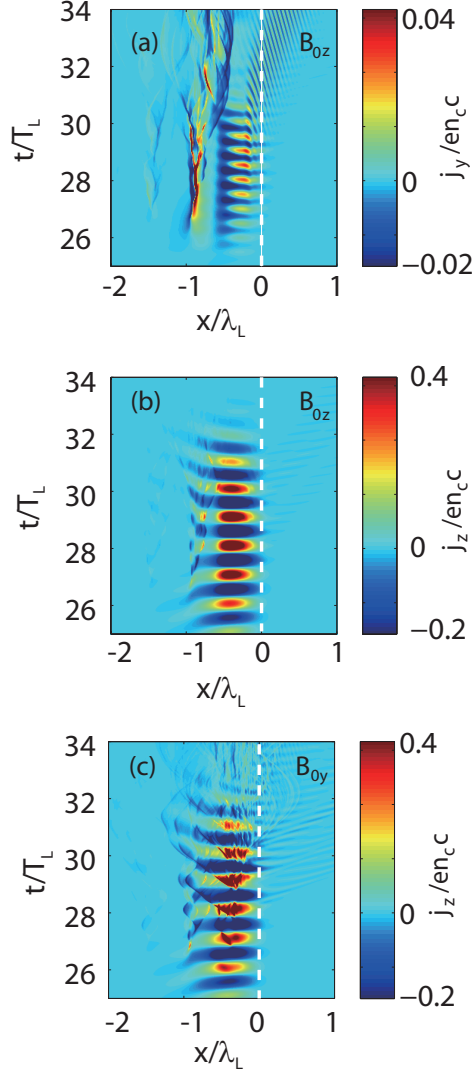


FIG. 3. (Color online) Space-time plots of electric current components j_y and j_z versus coordinate x and time t in units of λ_L and T_L with a magnetic field applied either in z - or y -directions. (a) and (b) are for j_y and j_z respectively with $B_{0z} = 17\text{MG}$, and (c) is for j_z with $B_{0y} = 17\text{MG}$. The dashed line shows the initial position of the critical plasma density.

is a kind of superposition of Fig. 3(a) and 3(b) and is dominated by the oscillation at ω_0 as expected.

Next we look into the dependence of this magnetic field induced even harmonic generation on the magnetic field strength and plasma density scalelength. Figure 4(a) shows a comparison of spectra for s and p -polarized reflected light. At the magnetic field strength of 17MG , the second harmonic due to B_{0y} is much weaker than that due to B_{0z} . However, with

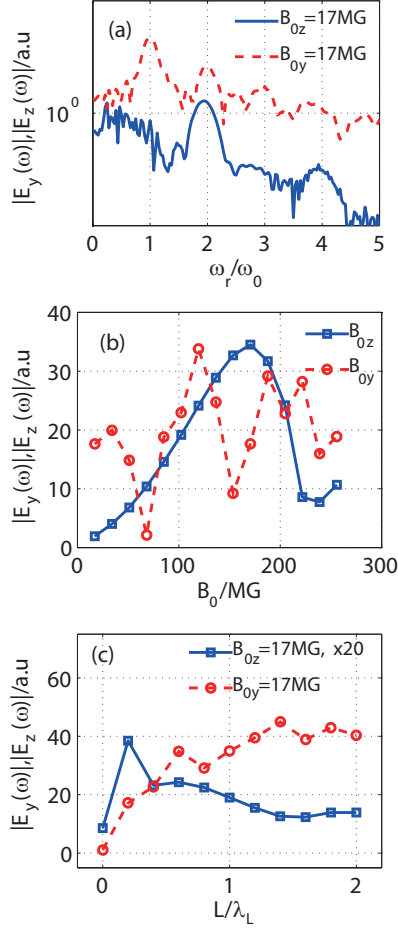


FIG. 4. (Color online) (a) The Fourier transformed spectra of E_y with the magnetic field $B_{0z} = 17\text{MG}$ (blue solid) and E_z with $B_{0y} = 17\text{MG}$ (red dashed) with $L = 0.2\lambda_L$. (b) Scalings of the 2nd harmonic spectra $|\text{FFT}(E_y)|$ (blue square) and $|\text{FFT}(E_z)|$ (red circle) with the strength of the magnetic field B_{0z} and B_{0y} , respectively, with $L = 0.2\lambda_L$. (c) Scalings of the 2nd harmonic spectra $|\text{FFT}(E_z)|$ (red circle) with $B_{0y} = 17\text{MG}$ and $|\text{FFT}(E_y)|$ (blue square, multiplied by 20) with $B_{0z} = 17\text{MG}$ with the preplasma length.

the increase of the magnetic field strength, it changes. As shown in Fig. 4(b), in a certain range ($<160\text{ MG}$), the spectral intensity of the second harmonic E_y depends linearly on the external magnetic field B_{0z} . It reaches the maximum at $B_{0z} = 160\text{MG}$ and weakens with stronger magnetic field. On the other hand, when applied with B_{0y} , there are several peaks in the second harmonic E_z as shown by the red circles in Fig. 4(b). This may be attributed to the much complicated coupling of cyclotron motion with both the longitudinal and transverse oscillations shown in Fig. 1(b). The almost linear scaling of the second harmonic

E_y with the magnetic field B_{0z} can be used to measure the magnetic field by detecting the emission of the second harmonics or higher even harmonics. A drive pulse can be used to generate the magnetic field near the critical density region and a probe pulse can be used to measure the field (Kahaly *et al.*, 2009). By changing the focusing positions and delay of the probe pulse, the distribution and temporal evolution of the magnetic field can be measured.

So far we have fixed the preplasma scalelength to be $L = 0.2\lambda_L$. The coupling efficiency also depends on the L employed. Figure 4(c) shows the correlation for the magnetic field strengths in both transverse directions with $B_{0z} = 17\text{MG}$ (blue) and $B_{0y} = 17\text{MG}$ (red). The preplasma scale of the target plays a crucial role in the surface oscillations. With the parallel magnetic field B_{0z} , the even harmonic intensity increases with the density scale length L when $L < 0.2\lambda_L$ and then decrease with the further increase of L . This is similar to the odd harmonics produced without the effect of magnetic field (Dollar *et al.*, 2013). With the perpendicular magnetic field B_{0y} , longer preplasma with $L > 0.2\lambda_L$ can produce even harmonics more efficiently. This suggests that the perpendicular magnetic field leads to higher coupling at long density scalelength.

Multi-dimensional effects

We also run three-dimensional (3D) PIC simulations to check possible multi-dimensional effects on this process. The simulation box is set to be $20 \times 20 \times 20\lambda_L^3$ in $x \times y \times z$ directions, with $64 \times 8 \times 8$ cells per wavelength. The plasma occupies a volume of $2 \times 18 \times 18\lambda_L^3$ with a sharp density front. An incident laser with a Gaussian transverse profile $a = a_0 \exp(-r^2/\sigma_0^2)$ is sent to the target from left, where $\sigma_0 = 2\lambda_L$ is the focal spot radius at waist. The other laser parameters are the same as in the 1D simulations with the laser field polarized along the z-direction. Despite much lower spatial resolutions compared with 1D simulation, they are fine enough to resolve the second harmonics.

A pair of comparison simulations are conducted, either with or without external magnetic field B_{0z} . Figure 5 shows the p polarized reflected fields for each case and their corresponding Fourier spectra in the $k - y$ space. It is seen that second harmonic generation occurs for both cases. For $B_{0z} = 0$, the harmonic is distributed in an annular pattern with a large divergence. This hollow harmonic is actually radial polarized and is probably caused by the transverse gradient of the incident laser pulse and plasma density as demonstrated in by

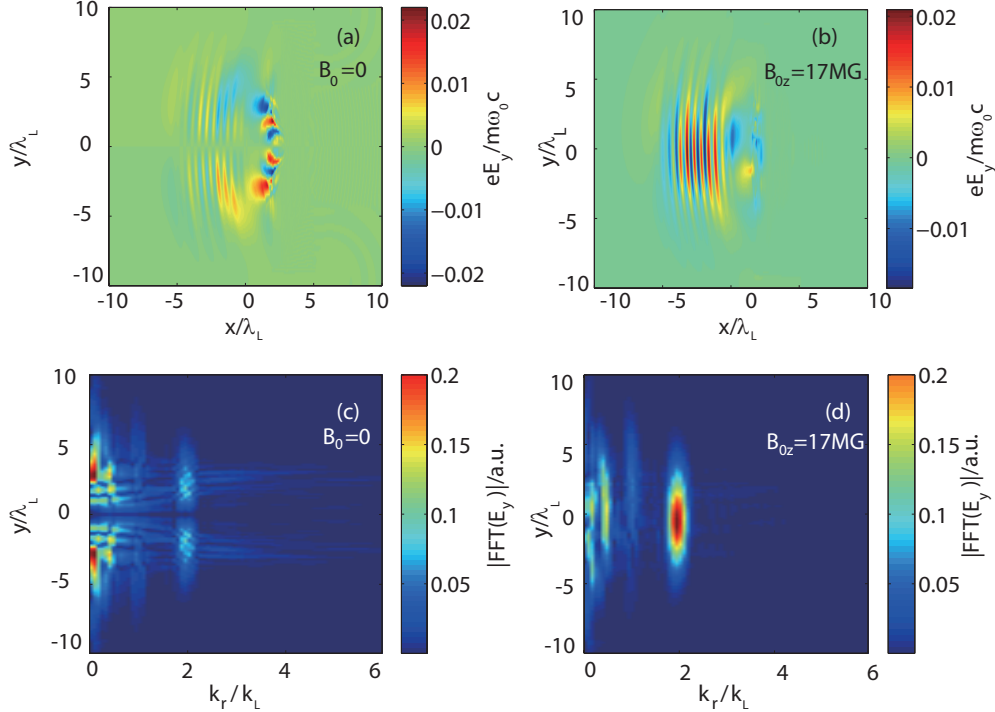


FIG. 5. (Color online) The results of 3D PIC simulations. The electric field E_y of the horizontal section at $z = 0$ in the magnetic field $B_{0z} = 0$ (a) and $B_{0z} = 17\text{ MG}$ (b). Plots (c) and (d) show the wave vector spectra $|\text{FFT}(E_y)|$ for the fields given in (a) and (b), respectively. The laser focal spot size is $2\lambda_L$.

(Gizzi *et al.*1996). While for the case of $B_{0z} = 17\text{MG}$, the even harmonics generally share the same Gaussian transverse profile as the drive pulse. This magnetic field induced even harmonic is much higher than that produced due to the transverse gradients of the incident laser pulse.

Laser spot size is a crucial parameter for routinely monitoring high intensity performance (Dromey *et al.*, 2009). If the laser has a large spot size, the situation is similar to 1D simulation. When the laser spot size is smaller, multi-dimensional effects such as hole boring will play a significant role and results in decrease of even order harmonics. To show this, we carry out two-dimensional (2D) simulations, with similar laser and plasma parameters as in 3D simulations. The spectral intensity of the second harmonics with $B_{0z} = 17\text{MG}$ is shown to increase with the laser focal spot size, and reaches saturation at $\sigma_0 = 3\lambda_L$. Similar results are found with the third harmonics with $B_{0z} = 0$, as shown in Fig. 6. With a small laser spot size, the oscillating mirror is not a perfect planar mirror as usually

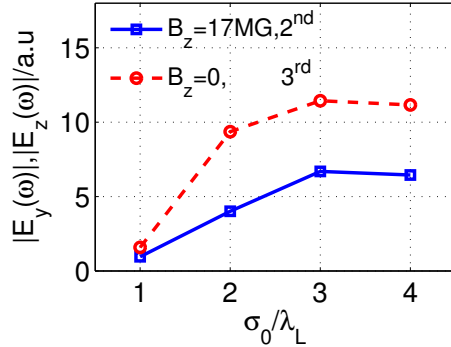


FIG. 6. (Color online) Scaling of spectral intensity of the second harmonic $|\text{FFT}(E_y)|$ (for $B_{0z} = 17\text{MG}$) and third harmonic $|\text{FFT}(E_z)|$ (for $B_{0z} = 0$) with the laser focal spot size obtained in two-dimensional simulations. The electron density is steep at the surface.

found in 1D simulation, due to hole boring effect. The reflected pulse also experiences diffraction spreading transversely, leading to decaying of the harmonic radiation quickly with the increase of distance away from the target surface. The second harmonic generated with $B_{0z} = 0$ is distributed more diversely with increasing σ_0 , with the amplitude and spectral intensity increasing at first and reaching saturation at $\sigma_0 = 3\lambda_L$, beyond which it decreases.

CONCLUSION

In conclusion, it is shown that external transverse magnetic field can change the parity of harmonics generated from laser-irradiated solid surface by modifying the coupling of the transverse and longitudinal oscillations of electrons at the solid surface. In particular, with even harmonics can be produced with different polarization from the driving laser pulse. The coupling of the electron cyclotron motion and the longitudinal oscillations at the second harmonic of the driving laser is responsible for the even harmonics generation. The results are confirmed by PIC simulations. The spectral intensity of the second harmonics depends linearly on the magnitude of the magnetic field parallel to the laser electric field, providing a way to measure the strong self-generated magnetic field during the laser-plasma interaction. The dependence of the second harmonic on the preplasma scale length is shown to increase with longer preplasma scale, in which may also be useful to evaluate the preplasma scalelength. Finally, both the magnetic field induced second harmonic and normal

third harmonic tend to increase with the laser spot size. When the latter is larger than $3\lambda_L$, the radiation fields become saturated. Additional even harmonic component generated due the transverse gradient of the incident laser pulse is found, which has radial polarization and emits with a conical distribution and is therefore distinctly different from the even harmonics induced by the magnetic field.

Z.M.S. would like to acknowledge the OSIRIS Consortium, consisting of UCLA and IST (Lisbon, Portugal) for the use of OSIRIS and the visXD framework. This work is supported by the National Science Foundation of China (11374210 and 11421064), a MOST international collaboration project (2014DFG02330) and a Leverhulme Trust Research Grant. Simulations were performed on the II supercomputer at Shanghai Jiao Tong University and on the Magic Cube II supercomputer of Shanghai High Performance Computing Center. [↵](#)